

# Intermittency Spectra of the Magnetic Field in Solar Active Regions

Valentyna Abramenko and Vasyl Yurchyshyn  
Big Bear Solar Observatory, 40386 N. Shore Lane, Big Bear City, CA 92314

## ABSTRACT

We present results of a study of intermittency and multifractality of magnetic structures in solar active regions (ARs). Line-of-sight magnetograms for 214 ARs of different flare productivity observed at the center of the solar disk from January 1997 until December 2006 are utilized. Data from the Michelson Doppler Imager (MDI) instrument on-board the *Solar and Heliospheric Observatory* (SOHO) operating in the high resolution mode, the Big Bear Solar Observatory digital magnetograph and *Hinode* SOT/SP instrument were used. Intermittency spectra were derived via high-order structure functions and flatness functions. The flatness function exponent is a measure of the degree of intermittency. We found that the flatness function exponent at scales below approximately 10 Mm is correlated to the flare productivity (the correlation coefficient is - 0.63). *Hinode* data show that the intermittency regime is extended toward the small scales (below 2 Mm) as compared to the MDI data. The spectra of multifractality, derived from the structure functions and flatness functions, are found to be more broad for ARs of highest flare productivity as compared to that of low flare productivity. The magnetic structure of high-flaring ARs consists of a voluminous set of monofractals, and this set is much richer than that for low-flaring ARs. The results indicate relevance of the multifractal organization of the photospheric magnetic fields to the flaring activity. Strong intermittency observed in complex and high-flaring ARs is a hint that we observe a photospheric imprint of enhanced sub-photospheric dynamics.

*Subject headings:* Sun: activity - Sun: flares - Sun: photosphere - Sun: surface magnetism - Physical Data and Processes: turbulence

## 1. Introduction

Energy release processes in solar active regions (ARs) could be, in general, divided into two types. The first one is a quasi-stationary energy release, which is responsible, for

example, for heating of ARs and manifests itself as continuous soft X-ray and ultra-violet emissions above an AR. It is well known that the total magnetic flux and the area of an AR are very well correlated with the total soft X-ray luminosity (Fisher et al. 1998). Contributions from adjacent domains of an AR are summed in the total X-ray luminosity. In this sense, the process might be considered as an additive, i.e., a linear process. Forecasting of such a process is straightforward and reliable.

Another type of energy release is an impulsive process known as solar flares of various energy scales: from nano-flares ( $10^{24}$  ergs) to super-strong eruptions of  $10^{33}$  ergs (see, e.g., Shimizu & Tsuneta 1997). A drastically different situation is encountered here. The physical background for the flare origin is a non-linear process occurring in a large volume ranging from the convective zone to the corona. Non-linear processes are multiplicative in nature and involve inter-scale energy exchange, in other words, a non-linear energy cascade. This is a way of evolution of any turbulent medium. Large fluctuations in temporal and spatial domains are not rare and they contribute significantly into the main values. The temporal and spatial images of the system (an AR in our case) acquire an intermittent (or, in other words, multifractal) character. Strictly speaking, in such a system, it is impossible to exactly predict the location and time of next large fluctuation (a solar flare in our case). However, since solar eruptions play a key role in Earth space weather, numerous empirical approaches were proposed during the last two decades to forecast solar flaring activity (see, e.g., the recent reviews by McAteer et al. 2009 and Georgoulis 2010 and references in).

In the present study, we do not offer yet another approach for solar flare prediction. We will rather focus on non-linearity and complexity as a function of spatial scales in solar magnetic fields - an environment hosting flares and, in many senses, responsible for flare activity in ARs. It is well known that a non-linear system can not be characterized adequately by only one scalar parameter. To explore the inter-scale energy exchange, we should consider various spectral functions of the system. Therefore, we focus here on intermittency and multifractality spectra of the photospheric magnetic field in various active regions displaying different flare productivity.

## 2. Data

A set of line-of-sight magnetograms, recorded for 214 ARs from January 1997 until December 2006, was analyzed. The bulk of the magnetograms (212) were obtained with the SOHO/MDI instrument (Scherrer et al. 1995) in the high resolution mode (MDI/HR, the pixel size of  $0.6''$ ). Data for two ARs (NOAA 9393 and 10720) were obtained with the Big Bear Solar Observatory's Digital Magnetograph (BBSO/DMG, Spirock 2005) at very

good seeing conditions (pixel size of  $0.6''$ ). For NOAA AR 10930, we also utilized *Hinode* line-of-sight magnetograms derived with the SOT/SP instrument (Tsuneta et al. 2008). In all of the cases, the region of interest was located near the solar disk center (no farther than  $20^\circ$  away from the central meridian), so that the projection effect was negligible.

ARs selection was performed for this study. First, only those ARs which were located inside the MDI/HR field-of-view (FOV) were analyzed. This requirement results in excluding of a large number of high-latitude ARs. And gaps in the MDI/HR data coverage diminished out data set. Second, a threshold on the total flux of an AR in question should be specified, otherwise there is no limit where to stop. For example, ephemeral active regions (e.g., Harvey & Martin 1972, total flux of about  $10^{20}$  Mx) are also active regions, although not associated with strong flaring. Magnetic structures of small compact ARs are usually purely resolved by MDI. Thus, to be consistent and analyze all ARs with the compatible quality, we have to select only ARs with total flux exceeding some threshold value. As a good compromise between the quality of analyzed data and the data set size, we chose this threshold value as  $10^{22}$  Mx. The total flux was calculated as a sum of absolute values of flux densities in all pixels of the magnetogram. For each AR, we analyzed one magnetogram.

The flare productivity of an AR was measured by the flare index,  $A$ , introduced in Abramenko (2005a). Since the X-ray classification of solar flares (X, M, C, and B) is based on denary logarithmic scale, we can define the flare index as

$$A = (100S^{(X)} + 10S^{(M)} + S^{(C)} + 0.1S^{(B)})/t. \quad (1)$$

Here,  $S^{(j)}$  is the sum of all GOES flare magnitudes of a certain X-ray class:

$$S^{(j)} = \sum_{i=1}^{N_j} I_i^{(j)}, \quad (2)$$

where  $N_j = N_X, N_M, N_C$  and  $N_B$  are the numbers of flares of X, M, C and B classes, respectively, that occurred in a given active region during its passage across the solar disk that is represented by the time interval  $t$  measured in days.  $I_i^{(j)} = I_i^{(X)}, I_i^{(M)}, I_i^{(C)}$  and  $I_i^{(B)}$  are GOES magnitudes of X, M, C and B flares. Interval  $t$  was taken to be  $27/2$  days for the majority of the ARs with exception of emerging ones. In general, those ARs that produced only B and C-class flares have the flare index smaller than 2, whereas several X-class flares will result in the flare index exceeding 100. Zero flare index does not indicate the absence of any flares. It rather means that our tools are not capable to detect extremely weak flares for a given AR. Again, in view of a question "where to stop", we chose to restrict ourselves by ARs of non-zero flare index as it was measured from the GOES data on the basis of Eqs. (1 - 2). Therefore, the flare index,  $A$ , analyzed here, represents an average rate of the flare

productivity of an ARs during the time interval of the AR’s presence on the solar disk, but not the probability of imminent flare.

Thus, our data set by no means is a complete one. It rather includes ARs in the tail of an ARs distribution (e.g., Zhang 2010) - a subset of ARs with moderate and large total flux and non-zero flare productivity. However, it is exactly these kind of events that define the space weather.

We note that, to some extent, the flare index may be considered to be a measure of intermittency in the *time* domain. Indeed, each flare in the time profile of integrated solar X-ray emission represents a strong fluctuation above the nearly continuous background of much weaker fluctuations. This description is in a perfect agreement with the definition of intermittency. Along with this, more rigorous measures for the temporal intermittency for ARs were suggested (see, e.g., Abramenko et al. 2008).

### 3. Intermittency Spectra: Method

There are many approaches to probe intermittency and multifractality (see, e.g., recent review by McAteer et al. 2009 for applications to the solar magnetic fields). We traditionally utilize the high-order structure functions approach (Stolovitzky & Sreenivasan 1993; Frisch 1995; Consolini et al. 1999; Abramenko et al. 2002, 2003, 2008; Abramenko 2005b, 2008; Georgoulis 2005; Buchlin et al. 2006; Uritsky et al. 2007).

Structure functions were introduced by Kolmogorov (1941) (the original Russian paper was later republished as Kolmogorov 1991) and are defined as statistical moments of the  $q$ -powers of the increment of a field. In our case, the analyzed field is the LOS component of the photospheric magnetic field,  $B_l$  (see Figure 1 for illustration), so the corresponding structure function can be written as

$$S_q(r) = \langle |B_l(\mathbf{x} + \mathbf{r}) - B_l(\mathbf{x})|^q \rangle, \quad (3)$$

where  $\mathbf{x}$  is the current pixel on a magnetogram,  $\mathbf{r}$  is the separation vector between any two points used to measure the increment (see the lower right panel in Figure 1), and  $q$  is the order of a statistical moment, which takes on real values. Here angular brackets denote averaging over the magnetogram, and the vector  $\mathbf{r}$  is allowed to adopt all possible orientations,  $\theta$ , from  $0^\circ$  to  $180^\circ$  (because of the absolute value of the increment in Eq. 3). The next step is to calculate the scaling of the structure functions, which is defined as the slope,  $\zeta(q)$ , measured inside some range of scales where the  $S_q(r)$ -function is linear and the field is intermittent. The function  $\zeta(q)$  is shown in the upper right panel in Figure 1.

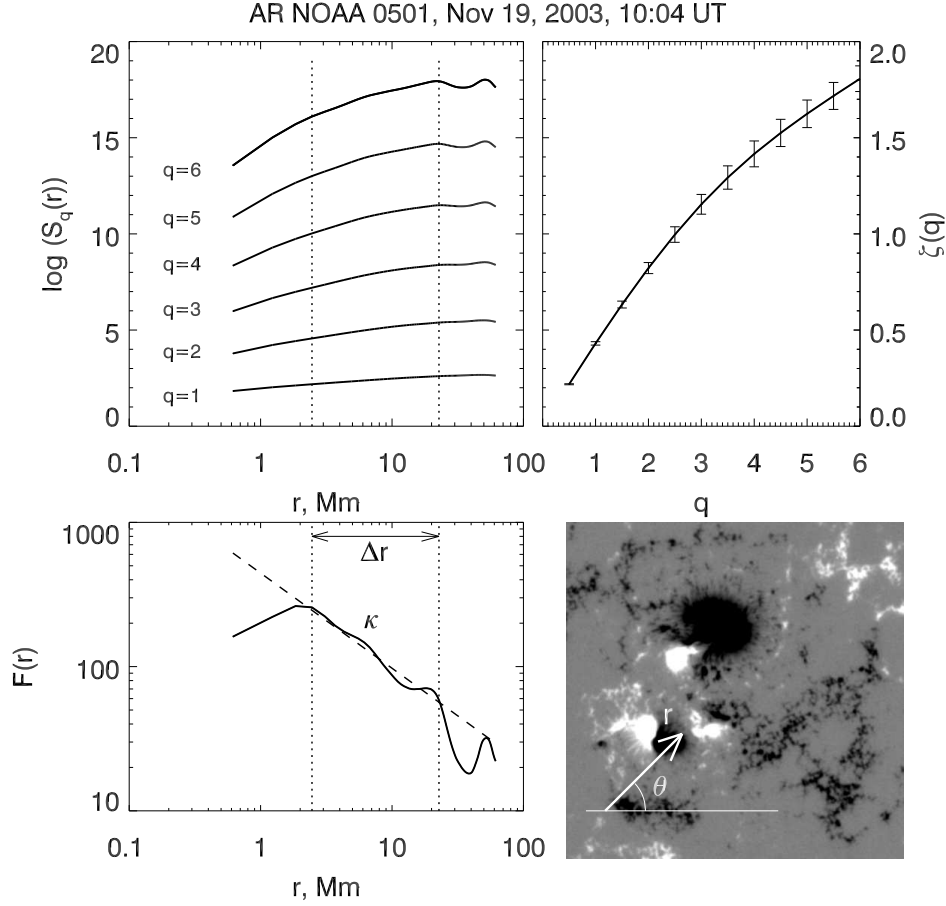


Fig. 1.— Structure functions  $S_q(r)$  (*upper left*) calculated from a magnetogram of active region NOAA 0501 (*lower right*) according to Equation (3). *Lower left* - flatness function  $F(r)$  derived from the structure functions using Equation (4). Error bars for  $S_q(r)$  and  $F(r)$  are no larger than the thickness of the lines, due to large statistics in Eq. 3. Vertical dotted lines in both left panels mark the interval of intermittency,  $\Delta r$ , where flatness grows as power law when  $r$  decreases. The index  $\kappa$  is the power index of the flatness function determined within  $\Delta r$ . The slopes of  $S_q(r)$ , defined for each  $q$  within  $\Delta r$ , constitute  $\zeta(q)$  function (*upper right*), which is concave (straight) for an intermittent (non-intermittent) field. An example of a separation vector  $\mathbf{r}$  and the corresponding directional angle  $\theta$  between the positive direction of the  $x$ -axis (EW-axis) and the vector  $\mathbf{r}$  (see Section 5 for further discussion) are shown on the magnetogram.

A weak point in the above technique is the determination of the range,  $\Delta r$ , where the slopes of the structure functions are to be calculated. To visualize the range of intermittency,  $\Delta r$ , we suggest to use the flatness function (Abramenko 2005b), which is determined as

the ratio of the fourth statistical moment to the square of the second statistical moment. To better identify the effect of intermittency, we followed Frisch (1995) and reinforced the definition of the flatness function and calculated the hyper-flatness function, namely, the ratio of the sixth moment to the cube of the second moment:

$$F(r) = S_6(r)/(S_2(r))^3 \sim r^{-\kappa}. \quad (4)$$

For simplicity, we will refer to  $F(r)$  as the flatness function, or intermittency spectrum. In case of a non-intermittent structure, the flatness function is not dependent on the scale,  $r$ . On the contrary, for an intermittent structure, the flatness grows as power-law, when the scale decreases. The slope of flatness function,  $\kappa$ , determined within  $\Delta r$ , i.e., the flatness function exponent, characterizes the degree of intermittency.

The index  $\kappa$  was computed from the best linear fit within  $\Delta r$  in the double logarithmic plot via the IDL/LINFIT routine by minimizing the  $\chi$ -square error statistic. This procedure was repeated for varying boundaries of  $\Delta r$ , and a range was determined where the best fit to the data points has the minimal standard deviation (a range of best linearity). Thus found range was gradually extended until the change in  $\kappa$  and standard deviation exceed 5%. This final interval was adopted as  $\Delta r$ .

#### 4. Intermittency spectra for various ARs

Analysis of  $F(r)$  functions for various ARs reveals that each AR exhibits a unique spectrum. The best way to sort them out was to start with simplest and well defined magnetic structures, such as unipolar spots. Our data set contained 38 unipolar sunspots of different size and polarity. Figure 2 shows magnetograms and flatness functions for three typical unipolar sunspots. The well pronounced smooth maximum in the flatness function near  $r_{max} \approx 10$  Mm is present for all 38 cases. As is evident from Figure 3, the scale, where the maximum is located, is well correlated with the size of a unipolar sunspot,  $d$ . The data points are predominantly located below the bisector of the diagram, so that the sunspot diameter is slightly larger than the scale  $r_{max}$ . The most plausible reason for that is the saturation effect inside strong sunspots in the MDI magnetograms, which artificially reduces the size of the largest magnetic structure and affects calculations of the structure functions at the scale of the sunspot size. On the other hand, measurements of the sunspot diameter are not affected by the saturation effect. According to the definition of intermittency (a structure where rare strong fluctuations are intermittent with vast areas of low fluctuations), the presence of an individual sunspot can produce the detectable effect of intermittency at scales of the sunspot size. Indeed, when we excluded the sunspot area from calculations of

the structure functions, the maximum disappears. Therefore, the appearance of the smooth maximum in  $F(r)$  of unipolar sunspots is caused by intermittency introduced by the only strong large sunspot seen in the image.

The positive slope in  $F(r)$  at scales smaller than  $r_{max}$  (see dashed segments in right panel of Figure 2) indicates the transition from the intermittent regime at scales above  $r_{max}$  to the non-intermittent regime, with nearly flat  $F(r)$  at scales  $r \ll r_{max}$ . It is natural that the non-intermittent regime cannot set in abruptly, so that some transition region appears (as it always does in spectral functions, see, e.g., Frisch 1995). The most important fact for us here is that there is no *negative* slope in  $F(r)$  at  $r < r_{max}$ , which can be interpreted as an absence of intermittency. A plateau at small-scales is lower for lower degree of intermittency. Therefore, the value of the *positive* slope of  $F(r)$  in the transition region is in opposite proportion to the degree of intermittency at small scales.

When analyzing more complex ARs, one might expect the presence of a local maximum in  $F(r)$  at scales of about 10-20 Mm, which appears to be a manifestation of large-scale intermittency introduced by strong isolated sunspots. We determined the diameter,  $d$ , of the largest sunspot (as an average half-width of  $B_l$  crosscut made in two orthogonal directions across the sunspot center) in each AR and then found the closest local maximum in  $F(r)$  and adopted it as  $r_{max}$  (see Figure 4, middle and bottom rows). When there was no local maximum, we accepted  $r_{max} = d$  (Figure 4, top row). We consider the position of  $r_{max}$  as a boundary between the large-scale intermittency (related to the presence of strongest sunspots) and small-scale intermittency (related to the internal magnetic complexity in an AR), and we use it below.

Flatness functions for ARs, which are more complex than unipolar sunspots, showed an undulating behavior and presence of negative-slope regions,  $\Delta r$ , at scales below  $r_{max}$  (see Figure 4 for typical examples). In this case, intermittency at scales within the range  $\Delta r$  is not defined by the presence of large sunspots but is rather caused by smaller-scale complexity associated with small sunspots and  $\delta$ -structures, strong gradients along numerous neutral lines, channel-like structures in the magnetic field, etc. Also, we note a tendency that in more complex ARs the intermittency interval and the steepness of the spectrum become larger.

We found 12 ARs, for which the flatness function was extremely steep and closely followed power law at all scales below 40-70 Mm down to 2-5 Mm. Examples of extremely intermittent cases are shown in Figure 5, where very broad ranges of steep power-laws in  $F(r)$  are evident, which is typical for highly intermittent structures (Frisch 1995). These ARs are the most complex in our data set and frequently they represent large  $\delta$ -structure active regions.

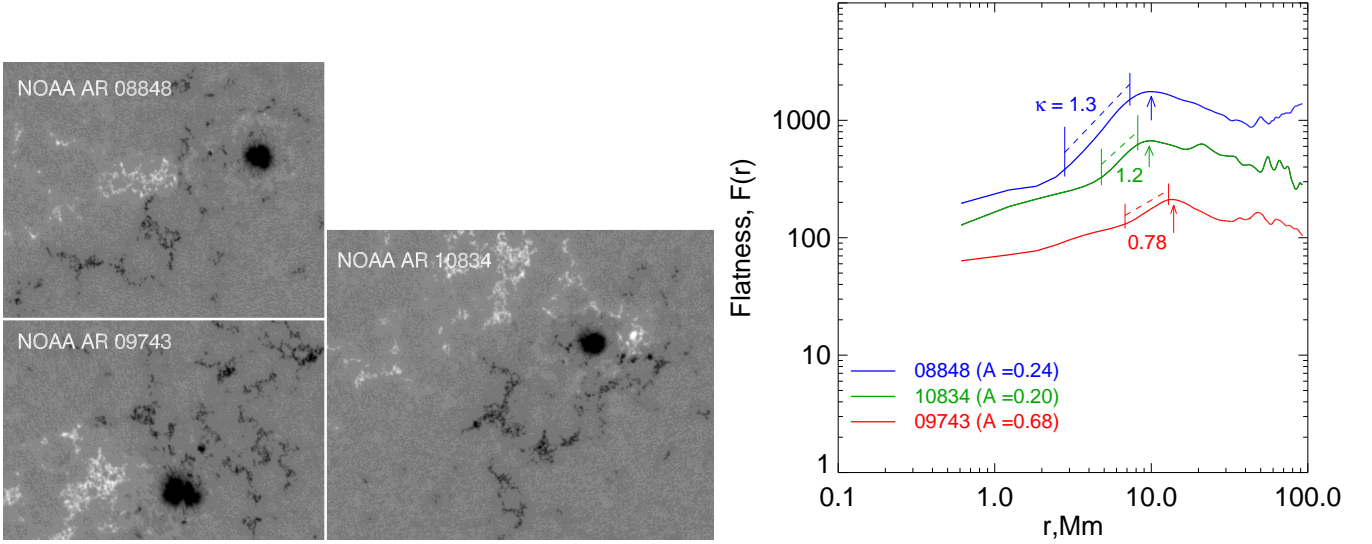


Fig. 2.— MDI/HR magnetograms for three unipolar sunspots groups (*left*) and the corresponding flatness functions (*right*). All magnetograms have the same spatial scale, and the width of NOAA AR 09743 magnetogram is 180 Mm. Flare index,  $A$ , is shown for each AR. All flatness functions display a well pronounced maximum at scales  $r_{max}$  (indicated with arrows), roughly corresponding to the size of a unipolar sunspot. The flatness exponent,  $\kappa$ , was determined from data points within the dashed line segments.

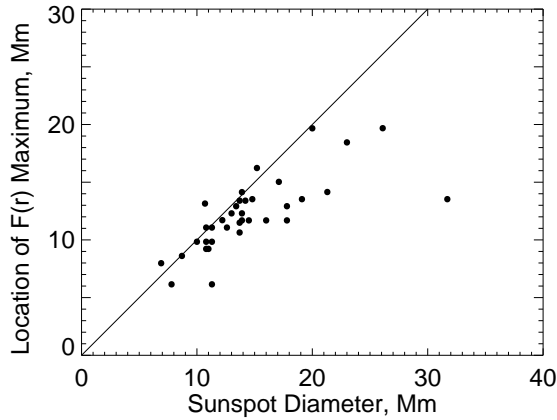


Fig. 3.— The spatial scale of the maximum,  $r_{max}$ , in the flatness function plotted versus the diameter,  $d$ , of unipolar sunspots. The solid line is the bisector.

## 5. Intermittency Index versus Flare Index

In Figure 6 (*left*) we related the flatness exponent,  $\kappa$ , with the flare index for 12 ARs of highest intermittency and for 38 non-intermittent ARs - unipolar sunspots. The



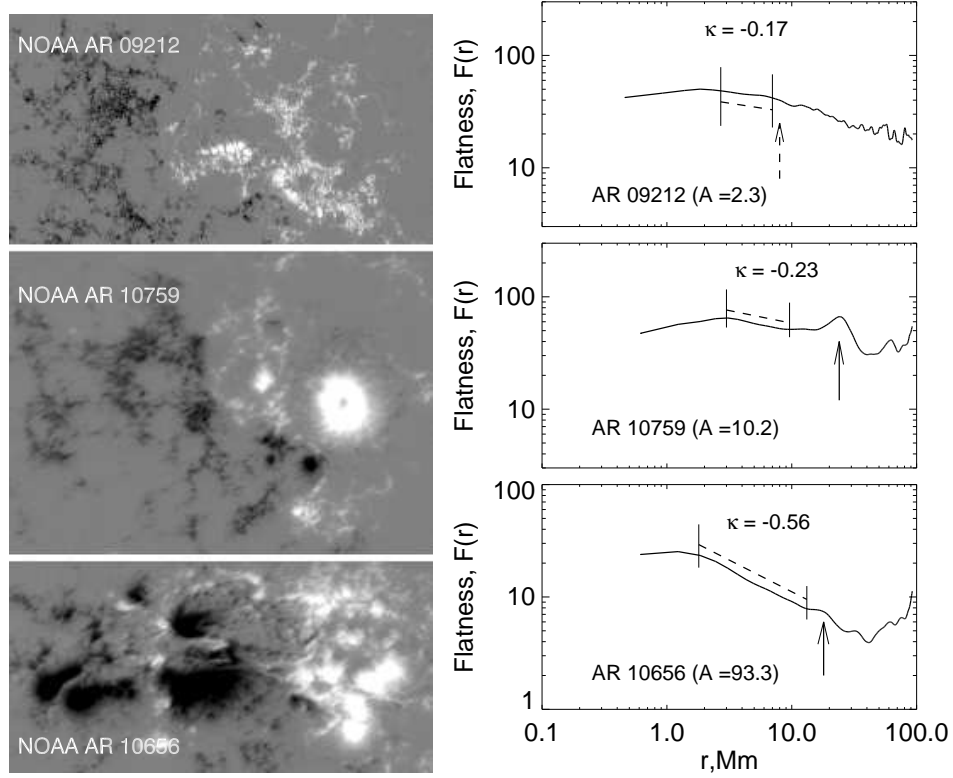


Fig. 4.— MDI/HR magnetograms for three active regions (*left*) and the corresponding flatness functions (*right*). The widths of the magnetograms (from top to bottom) correspond to 290, 170, 183 Mm. The dashed arrow marks a locations of  $r_{max}$  derived as a size of the largest sunspot. Other notations are the same as in Figure 2.

non-intermittent ARs (green circles) display very low flare productivity, whereas the ARs of highest intermittency (red circles) all are associated with very high flare index. the Pearson correlation coefficient is  $-0.83$  (with the 95% confidence interval of  $0.79 - 0.87$  according to the Fisher’s Z-transformation statistical test of significance<sup>1</sup>). Thus, the non-intermittent and highly-intermittent ARs are prone to display low and high flare productivity, respectively.

The right panel in Figure 6 is a combined plot for all ARs. The tendency here is the same: higher degree of intermittency corresponds to stronger flare productivity. For all ARs, the Pearson correlation coefficient is  $-0.63$  with the 95% confidence interval of  $0.54 - 0.70$ .

<sup>1</sup><http://icp.giss.nasa.gov/education/statistics/page3.html>

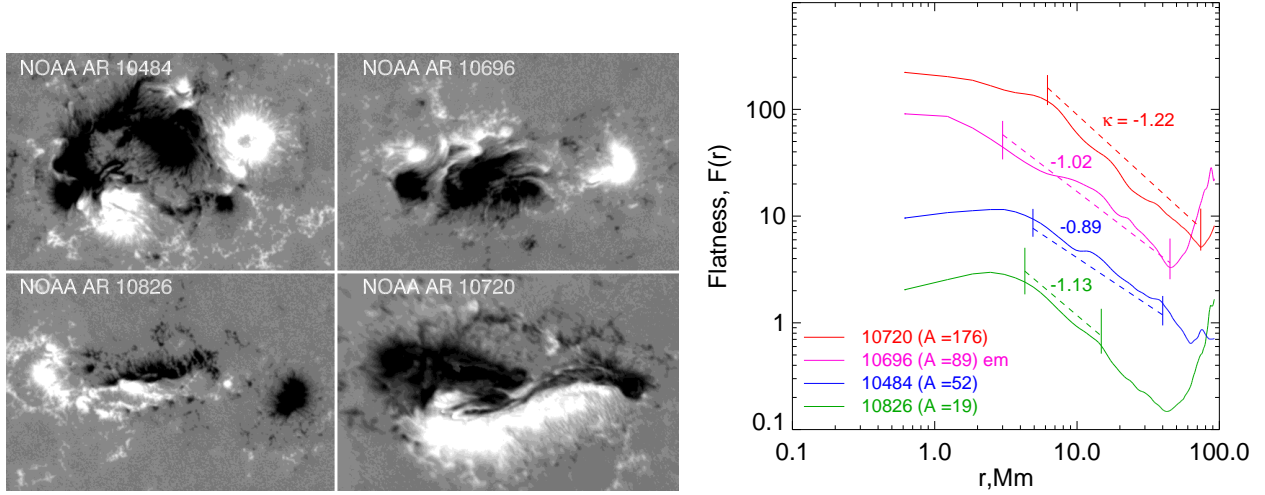


Fig. 5.— MDI/HR magnetograms (*left*) and flatness functions (*right*) for four ARs with the most pronounced intermittency at small scales.  $F(r)$  functions are shifted along the  $Y$ -axis into "well-readable" positions. The dashed line segments mark ranges of small-scale intermittency. Flare index,  $A$ , and exponents  $\kappa$  are indicated for each AR. All magnetograms have the same spatial scale, and the width of the AR NOAA 10484 magnetogram is 165 Mm.

Apart from our data set of 214 flaring ARs, there was a subset of 34 ARs (also observed during 1997-2006) for which the total flux exceeded the threshold value of  $10^{22}$  Mx while the respective flare index was zero. Most of them were unipolar sunspot groups. We find that their flatness function exponent,  $\kappa$ , is in the range of 0 - 1.5 which is practically the same as that for low-flaring ARs. Future observations with better flare and flux sensitivity might change the right-hand part of the diagram in Figure 2b, but not much changes are expected for the top-left part of the diagram.

We also compared the flare index versus the slope of the spectrum at scales *exceeding*  $r_{max}$  and obtained a very low correlation ( $CC = -0.25$  with the 95% confidence interval of 0.12 - 0.37). Therefore, the intermittency at large scales hardly contributes to the flare productivity of an AR. It rather indicates the presence of dominant sunspots in the AR. To the contrary, small-scale intermittency (at scales  $r < r_{max}$ ) seems to be essentially related to the AR's flaring rate. Further we will discuss intermittency only at small scales.

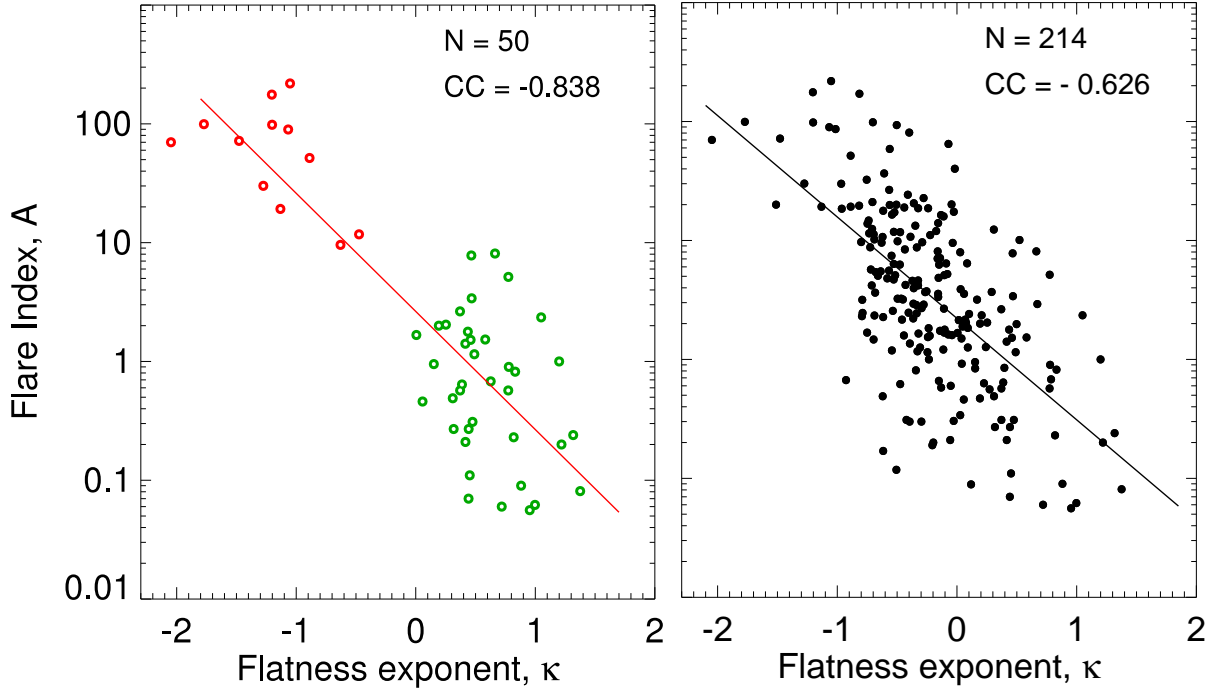


Fig. 6.— *Left* - The flare index,  $A$ , plotted versus the flatness exponent,  $\kappa$ , for 12 ARs of the most steep and extended intermittency spectra (red circles) and for 38 non-intermittent ARs (green circles). *Right* - The same but for all ARs in the data set.

## 6. Flatness Functions from MDI/HR and Hinode SOT/SP Magnetograms

We compared flatness functions for NOAA AR 10930 derived with SOHO/MDI and Hinode/SOT/SP magnetographs observed on December 11, 2006 (Figure 7). The level2 SP magnetograms were processed with HAO’s MELANIE code. The data are available at <http://sot.lmsal.com/data/sot/level2hao-new>. At scales 2 - 10 Mm, the two functions are in good agreement. At scales below 2 Mm, the MDI flatness functions saturate, while Hinode flatness functions show rapid increase with decreasing scale. The slope there is even steeper than it is inside the 2 - 10 Mm range, which indicates that intermittency might become stronger as the scale decreases and the spatial resolution improves. Note that the increase of the Hinode resolution results in the steepening of the flatness function at small scales. This comparison shows that the saturation in the MDI functions is caused by low sensitivity and resolution of an instrument rather than by absence of intermittency at small scales.

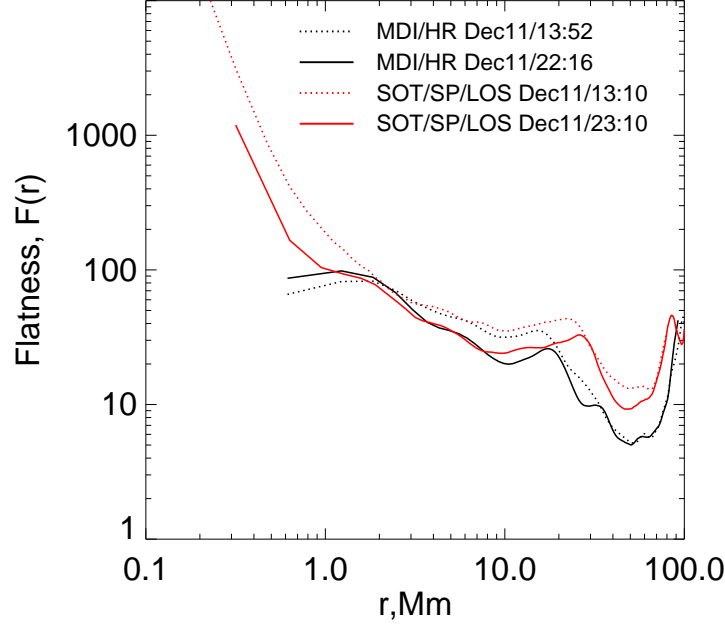


Fig. 7.— Flatness functions calculated from two MDI/HR magnetograms (*black*) and two Hinode SOT/SP LOS magnetograms (*red*) for NOAA AR 10930. Dotted (solid) lines refer to the magnetograms taken approximately 39 (27) hours prior to the X3.4 flare. The 13:10 SOT/SP magnetogram (*red dotted*) has a pixel size of  $0.148 \times 0.16''$  and shows the steepest growth of  $F(r)$  at small scales. The 23:10 SOT/SP magnetogram (*red solid*) has a pixel size of  $0.297 \times 0.32''$ .

## 7. Directional Structure Functions

As we indicated earlier, strong field gradients along a neutral line, small  $\delta$ -structures and shredded magnetic fields all can be plausible cause of strong small-scale intermittency. In attempt to clarify this assumption, we refined the calculation of the structure functions as described below.

According to the general definition of structure functions (see Section 3), functions  $S_q(r)$  produce an intermittency measure, which is averaged over all possible directions of the separation vector  $\mathbf{r}$ . To explore how the intermittency varies in different directions, we calculate directional structure functions, where the averaging in Eq. 3 is performed only over the separation vectors of a certain orientation,  $\mathbf{r}(\theta)$  (see lower right panel in Figure

1, the origin of  $\mathbf{r}$  is arbitrary). Specifying a set of bins for  $\theta$  ranging from  $0^\circ$  to  $180^\circ$  we calculated  $S_q(r, \theta)$  functions. We thus find that  $|\kappa(\theta)|$  varies significantly with  $\theta$ . Moreover,

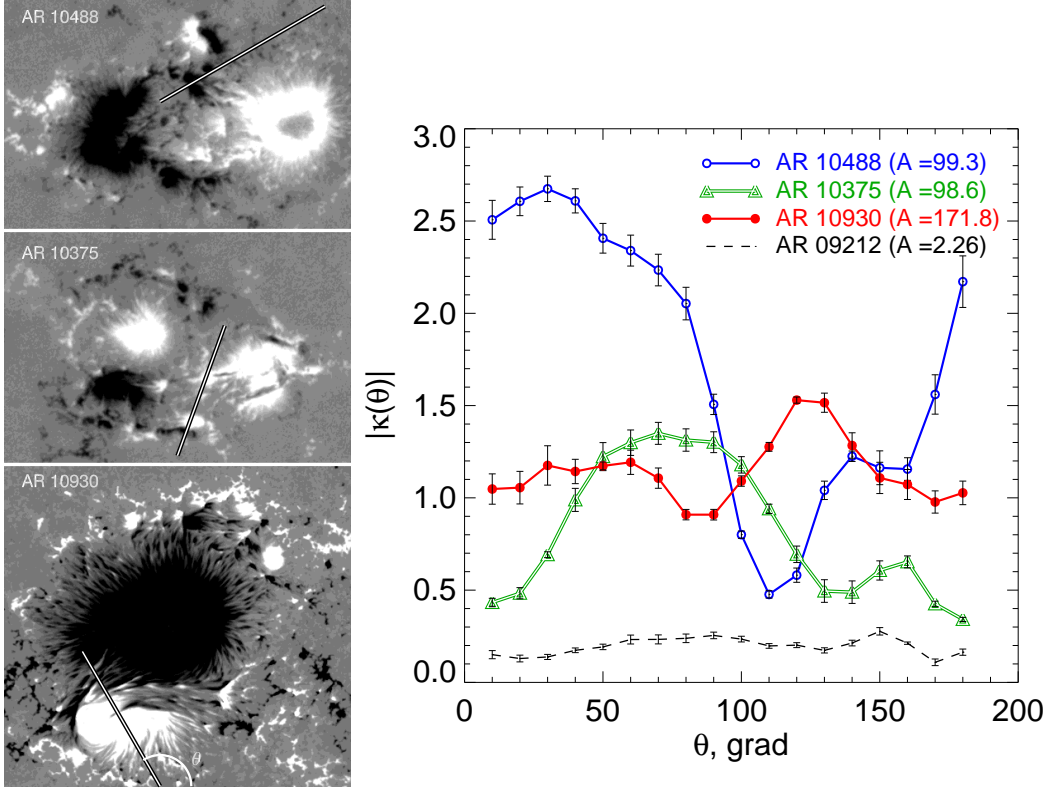


Fig. 8.— *Left* - MDI/HR magnetograms of NOAA ARs 10488 and 10375 (two top panels) and SOT/SP LOS magnetogram of NOAA AR 10930. All magnetograms are scaled between -800 and 800 G. North is to the top, west is to the right. The width of the MDI magnetograms is 152 Mm and SP magnetogram is 77 Mm. *Right* - Variations of the modulus of  $\kappa$  versus the directional angle,  $\theta$ , measured in the counter-clock-wise direction from the EW direction of the horizontal axis on the corresponding magnetogram. The orientation  $\theta(max)$ , where each function  $|\kappa(\theta)|$  peaks, is indicated with double line segments in the magnetograms. For the best view, the origins of segments are chosen so that the segments intersect the features of interest.

these fluctuations are particularly strong in the ARs showing strong flare productivity. Examples are shown in Figure 8. Thus, for NOAA AR 10488, the angle segment bounded by directions of  $0^\circ$  and  $70^\circ$  with the maximum at  $\theta(max) = 30^\circ$  is associated with much stronger intermittency as compared to other directions. When we plot this preferred direction ( $\theta(max) = 30^\circ$ ) on the magnetogram (double line segment in the upper left panel of Figure 8), we find that it crosses a set of small-scale extended threads and filament-like magnetic features connecting the two opposite polarity sunspots. Besides, it is also the

direction of the largest gradient across the small delta-structure in the northern part of the AR. Similar situation also appears in several other high-flaring ARs (Figure 8). We found more symmetric angular distribution of intermittency in ARs of low flare productivity. An example for AR NOAA 09212 is shown with a dashed line in Figure 8 (*right*).

## 8. Connection to the multifractality spectrum, $f(\alpha)$

The proposed technique to calculate flatness function,  $F(r)$ , also allows us to determine the intermittency interval,  $\Delta r$ . This interval appears to be the best appropriate interval to derive the slope,  $\zeta(q)$ , of the  $S_q(r)$  function. Indeed, scaling of the structure function should be determined at an interval where the field is intermittent. However, in very smooth  $S_q(r)$  functions, there is no a priori indications for such an interval (see Figure 1). It can, fortunately, be determined by using function  $F(r)$ : the intermittency interval is detected as a range where  $F(r)$  increases as a power law with decreasing scale. The slope of  $S_q(r)$ , derived inside  $\Delta r$  for each  $q$ , gives us  $\zeta(q)$  function (Figure 1, upper right panel).

For monofractals, function  $\zeta(q)$  is a straight line due to a global scale-invariance. And it has a concave shape in case of a multifractal. The degree of concavity is usually measured by function  $h(q) = \zeta(q)/dq$ . All values of  $h$ , within some range, are permitted for a multifractal, and for each value of  $h$  there is a monofractal with an  $h$ -dependent dimension  $D(h)$  at which the scaling holds with exponent  $h$  called the strength of singularity. This representation of multifractality is based on the increments of the field and has its roots in the theory of turbulence (Kolmogorov 1941). There exists another representation based on the dissipation,  $\varepsilon$ , of the field energy, which relies on the Kolmogorov’s (1941) result stating that field increments over a distance  $r$  scale as  $(\varepsilon r)^{1/3}$ , known as the refined similarity hypothesis (Monin& Yaglom 1975). In multifractal terminology the refined scaling hypothesis means that to any singularity of exponent  $\alpha$  of  $\varepsilon r$ , there is an associated singularity of exponent  $h = \alpha/3$  for the field of the same set, which has the same dimension  $D(h)$ . Usually, it is very difficult to measure the local dissipation in the 3D space. So, one-dimensional space averages of the dissipation are usually used. The corresponding dimension  $f(\alpha) = D(h) - (d - 1)$  has decreased by two units (for the space dimension  $d = 3$ ) because one-dimensional cuts of a 3D structure are taken. In the literature  $f(\alpha)$  is often referred as the multifractality spectrum (see, e.g., Feder 1988; Lawrence et al. 1993; Frisch 1995; Schroeder 2000; Conlon et al. 2008; McAteer et al. 2009). The values of  $D(h)$ , in turn, can be calculated as a Legendre transform of  $\zeta(q)$  (Frisch 1995):

$$D(h(q)) = \inf_q (d + qh(q) - \zeta(q)). \quad (5)$$

When  $\zeta(q)$  is concave, then for a given value of  $q$  (recall that  $q$  takes real values) the

extremum in Eq. 5 is attained at the unique value  $h_o(q)$ , and

$$D(h_o(q)) = d + qh_o(q) - \zeta(q). \quad (6)$$

We applied the above formulas for our case,  $d = 2$ . Examples of the multifractality spectra are shown in Figure 9. One can see that the most complex and flare-productive ARs (left frame in Figure 9) exhibit broader spectra as compared to that of low-flaring ARs. This means that a set of monofractals that form an observed multifractal, is much more broad in highly-flaring ARs as compared to low-flaring ARs. For comparison, in Figure 9 (right frame) we plot  $f(\alpha)$  calculated for a plage area. Flatness function for plage areas are linear in a broad range of scales, with small  $\kappa$ , - similar to that shown in Figure 4 (top right panel). However, the multifractality spectrum for them is rather narrow, similar to that for low-flaring ARs.

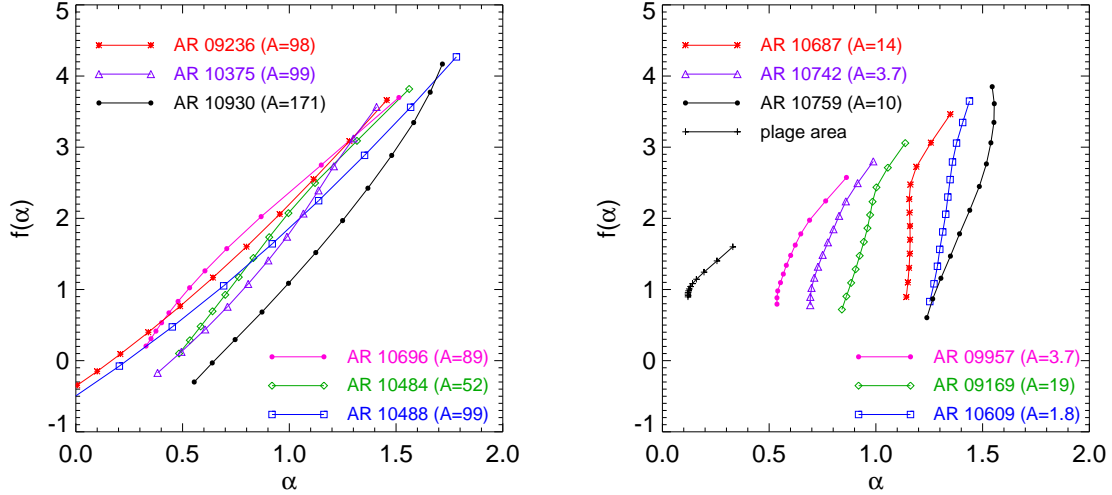


Fig. 9.— Multifractality spectra,  $f(\alpha)$ , plotted: *left* - for ARs of high flare productivity; *right* - for ARs of low flare productivity and for a plage area. Spectra on the left frame are more broad than that on the right frame.

## 9. Conclusions and Discussion

Analysis of intermittency and multifractality for magnetic structure in ARs allows us to conclude the following.

1. Intermittency at small scales is relevant to flare productivity. For the majority of ARs there is a smooth maximum in the intermittency spectrum at scales of  $r_{max} \approx 10$  Mm. The characteristic scale value  $r_{max}$  roughly corresponds to the size of dominant sunspots in an AR. Two intervals of intermittency on both sides of  $r_{max}$  were defined. Namely, large-scale intermittency at scales above  $r_{max}$ , and small-scale intermittency at lower scales. The large-scale intermittency is caused by the presence of strongest magnetic inhomogeneities - dominant sunspots. The degree of the large-scale intermittency does not correlate with flare productivity. The small-scale intermittency is present in all ARs except unipolar sunspots. The small-scale region of intermittency spectra is steeper for ARs of higher flare productivity. The correlation coefficient between the flare index and the index of the small-scale intermittency spectra is - 0.63.

2. In respect to the shape of intermittency spectra, all ARs could be divided into three types. The ARs of the first type (12 out of 214, most of them are  $\beta\gamma\delta$ -type ARs according to Mount Wilson classification) display a well-pronounced power-law steep spectrum in a broad range of scales,  $\Delta r$ : from 40-70 Mm down to 2-5 Mm. For some of them, there is no characteristic scale  $r_{max}$ , and the large-scale intermittency interval is smoothly connected to the small-scale intermittency interval. These ARs are very complex and the most flare productive. They also display the highest degree of intermittency as measured by the flatness exponent,  $\kappa$ , and the broadest multifractality spectrum,  $f(\alpha)$ , (see below).

The second type of ARs (164 of 214) are moderate active regions (most of them are  $\beta\gamma$ -type ARs). Their spectra usually display the  $r_{max}$ -peak followed by the moderate increase of  $F(r)$  at smaller scales. The flatness exponent in these ARs tends to be lower than that for the ARs of the previous type.

The third type of ARs (38 out of 214) do not display intermittency at scales  $r < r_{max}$ . All of these ARs are unipolar spots ( $\alpha$ -type ARs according to Mount Wilson classification) of very low flaring rate.

3. Analysis of directional intermittency spectra determined for various directions on a magnetogram showed that in flare productive ARs, angular variations of intermittency are highly inhomogeneous. There are angular segments where the degree of intermittency is highest, and these contribute significantly into the total amount of intermittency in an AR. These directions cut across the main direction of narrow magnetic filaments and/or along the largest gradients in a small  $\delta$ -structures present in an AR. In NOAA AR 10930, for example, this direction is nearly perpendicular to the magnetic filaments along the main neutral line separating two sunspots of the global delta-structure. We suggest that these small-scale shredded and stressed magnetic filaments are responsible for formation of small-scale intermittency and they are relevant to the high flare rate. This idea seems to be



in good agreements with Schrijver et al. (2008) who reported that in this particular event, a current-carrying twisted flux rope was responsible for the powerful X3.4 flare.

4. The important outcome of the above study is that the most flare-productive ARs tend to represent the most abundant multifractals. The multifractality spectra,  $f(\alpha)$ , show that ARs of highest flare productivity display the broadest range of multifractality (the range of singularity exponents,  $\alpha$  and  $h$ ). This further indicates that their magnetic structure consists of a voluminous set of monofractals, and this set is much richer than that for low-flaring ARs. Changes in the multifractality spectra during the AR's emergence were studied by Conlon et al. (2008). These authors found that noticeable changes in the spectra occur at the early, no-flaring, stage of emergence, whereas the beginning of flare activity is accompanied by the stabilization of the spectrum. This result also indicates relevance of the multifractal organization of the photospheric magnetic fields to the flaring activity.

5. As the resolution improves, the multifractality at small scales becomes more pronounced: Hinode SOT/SP magnetograms spectra become increasingly steeper as the spatial scale decreases. Thus, observations of ARs of the 24rd solar cycle with high resolution instruments, such as Hinode SOT, SDO/HMI, and Big Bear Solar Observatory New Solar Telescope (BBSO/NST, Goode et al. 2010) will bring new opportunities to study solar magnetism via the multifractality approach.

The intermittent/multifractal nature of the magnetic field in solar active regions attributes not *only* to the geometrical organization of the solar-surface magnetism as it might be assumed from the first sight. Indeed, on the contrary to a Gaussian process (where chaos is determined by a *sum* of numerous independent variables, and high-order statistical moments are fully determined by the first two moments), an intermittent process is rather a *product* of large number of independent variables when high statistical moments growth arbitrary with the number of the moment. These considerations, when converted to physics, imply that random strong peaks in the solution of the problem of the vector-field's transport by random flows (say, the magnetic field vector in a turbulent electro-conductive flow) correspond to structural features such as flux tubes and/or thin sheets of magnetic field lines. Strong intermittency observed in complex ARs is a hint that we observe a photospheric imprint of enhanced sub-photospheric dynamics.

Authors are thankful to Roberto Bruno, Vincenzo Carbone, Manolis Georgoulis, Philip Goode, James MsAteer, Jean-Claude Vial and Vadim Uritsky for helpful discussions and encouragement of this study. We are grateful to anonymous referee whose criticism and comments helped to improve the paper. SOHO is a project of international cooperation between ESA and NASA. Hinode is a Japanese mission developed and launched by ISAS/JAXA, collaborating with NAOJ as a domestic partner, NASA and STFC (UK)

as international partners. Scientific operation of the Hinode mission is conducted by the Hinode science team organized at ISAS/JAXA. This team mainly consists of scientists from institutes in the partner countries. Support for the post-launch operation is provided by JAXA and NAOJ (Japan), STFC (U.K.), NASA (U.S.A.), ESA, and NSC (Norway). Hinode SOT/SP inversions were conducted at NCAR under the framework of the Community Spectro-polarimetric Analysis Center (CSAC; [http : //www.csac.hao.ucar.edu/](http://www.csac.hao.ucar.edu/)). This work was supported by NSF grant ATM-0716512 and NASA LWS grant NNX08AQ89G.

## REFERENCES

- Abramenko, V. 2005a, ApJ, 629, 1141
- Abramenko, V. 2005b, Solar Phys., 228, 29
- Abramenko, V.I.: 2008, In: Wang, P.(ed), *Solar Physics Research Trends*, Nova Science Publishers, Inc., New York, 95.
- Abramenko, V., Yurchyshyn, V., Wang, H. & Goode, P. R. 2001, Sol. Phys., 201, 225
- Abramenko, V.I., Yurchyshyn, V.B., Wang, H., Spirock, T.J., Goode, P. R.: 2002, *Astrophys. J.* **577**, 487.
- Abramenko, V.I., Yurchyshyn, V.B., Wang, H., Spirock, T.J., Goode, P. R.: 2003, *Astrophys. J.* **597**, 1135.
- Abramenko, V.I., Yurchyshyn, V.B. & Wang, H. 2008, ApJ, 681, 1669.
- Buchlin, E., Vial, J.-C., Lemaire, P. 2006, A & A, 451, 1091.
- Conlon,P.A., Gallagher,P.T., McAteer,R. T. J., Ireland,J., Young,C. A., Kestener,P., Hewett,R. J., Maguire,K. 2008, Solar Phys., 248, 297
- Consolini, G., Berrilli, E., Pietropaolo, E., Bruno, R., Carbone, V., Bavassano, B., Ceppatelli, G. 1999, in: *Magnetic Fields and Solar Processes*, (ESA SP-448; Paris: ESA), 209.
- Feder, J. 1988, "Fractals", (New York:Plenum)
- Fisher, G.H., Longcope, D.W., Metcalf, T.R., Pevtsov, A.A. 1998, ApJ, 508, 885.
- Frisch, U. 1995, *Turbulence, The Legacy of A.N. Kolmogorov*, Cambridge University Press.

- Georgoulis, M. 2005, *Solar Phys.*, 228, 5.
- Georgoulis, M. 2010, *Solar Phys.*, in press.
- Goode, P. R., Yurchyshyn, V., Cao, W., Abramenko, V., Andic, A., Ahn, K., Chae, J. 2010, *ApJL*, 714, L31
- Harvey, K.L, Martin, S.F. 1973, *Solar Phys.* 32, 389
- Kolmogorov, A.N. 1941, *C.R. Acad. Sci. USSR*, 30, 301, republished as: Kolmogorov, A.N. 1991, *Proceedings of the Royal Society of London. Series A: Mathematical and Physical Science*, 434, 9.
- Lawrence, J. K., Ruzmaikin, A. A., Cadavid, A. C. 1993, *ApJ*, 417, 805
- McAteer, R.T.J., Gallagher, P.T., Conlon, P.A. 2009, *Adv. in Space Res.*, 45, Issue 9, 1067
- Monin, A.S., Yaglom, A.M. 1975, "Statistical Fluid Mechanics", vol. 2, ed. J.Lumley, MIT Press, Cambridge, MA
- Schrijver, C. J.; De Rosa, M. L.; Metcalf, T. and 14 co-authors 2008, *ApJ*, 675, 1637.
- Scherrer, P.H., Bogart, R.S., Bush, R.I., Hoeksema, J.T., Kosovichev, A.G., Schou, J., Rosenberg, W., Springer, L., Tarbell, T.D., Title, A., Wolfson, C.J., Zayer, I. and the MDI engineering team, 1995, *Sol. Phys.*, 162,129
- Schroeder, M. R. 2000, "Fractals, Chaos, Power Laws", New York:W.H. Freeman and Company
- Shimizu, T. & Tsuneta, S. 1997, *ApJ*, 486, 1045.
- Spirock, T.J. 2005, PhD thesis, New Jersey Institute of Technology.
- Stolovitzky, G., Sreenivasan, K.P. 1992, *Phys. Rev. E*, 48, R33.
- Tsuneta, S.; Ichimoto, K.; Katsukawa, Y.; Nagata, S.; Otsubo, M.; Shimizu, T.; Suematsu, Y.; Nakagiri, M.; Noguchi, M.; Tarbell, T.; Title, A.; Shine, R.; Rosenberg, W.; Hoffmann, C.; Jurcevic, B.; Kushner, G.; Levay, M.; Lites, B.; Elmore, D.; Matsushita, T.; Kawaguchi, N.; Saito, H.; Mikami, I.; Hill, L. D.; Owens, J. K. "The Solar Optical Telescope for the Hinode Mission: An Overview" *Solar Physics*, Volume 249, Issue 2, pp.167-196, 2008
- Uritsky, V. M., Paczuski, M., Davila, J. M., Jones, S. I. 2007, *Physical Review Letters*, 99, 025001.

Zhang, J 2010, American Astronomical Society, AAS Meeting 216, Abstract number 317.05